J. Coat. Technol. Res., **15** (3) 633–641, 2018
https://doi.org/10.1007/s11998-017-0012-9

Ultra-repellency of Al surfaces: design and evaluation

Y. Zhu, Y. M. Hu, L. Ma, H.-Y. Nie, W. M. Lau

Abstract Aluminum (Al) surfaces with ultra-repellency as well as desirable robustness were designed and fabricated. With photolithographic patterning of a thick SU-8 layer and sputtering of a thin Al film, re-entrant micro-pillar textured Al surfaces were prepared. After derivatization with perfluoroalkyl phosphoric acid (FPA), the textured Al surfaces showed ultra-repellency for a wide variety of liquids. The contact angles (CAs) of deionized (DI) water, hexadecane and dodecane were larger than 150°, and those of methanol and ethanol were larger than 100°. The sliding angles (SAs) of DI water, hexadecane and dodecane were 5°, 10°, and 10°, respectively, showing excellent superamphiphobicity. The SAs of methanol and ethanol were in the range of 20°–30°. The robustness of the ultra-repellent Al surface was evaluated by three parameters: robust height (H^*), robust angle (T^*) and robust factor (A^*). For the DI water probing, the values of the parameters are $H^* \approx 403$, $T^* \approx 119$ and $A^* \approx 92$, respectively, indicative of a desirable robustness. We clarified that only re-entrant structures can support composite liquid–solid–vapor interfaces when the corresponding Young's CAs are smaller than 90°, and the function of the nanometer structures of the hierarchical textures which were widely adopted to fabricate superamphiphobic surfaces is to help construct re-entrant structures. FPA derivatization is effective in lowering the surface energy of Al surfaces, combining with re-entrant textures to provide a simple and high throughput approach to ultra-repellency for a wide variety of liquids.

Keywords Ultra-repellency, Al surface, Re-entrant texture, PFA, Robustness

Introduction

Ultra liquid-repellency with contact angles (CAs) of liquid droplets placed on solid surfaces being larger than 150° for water and oils (superamphiphobicity), and 90° for alcohols, together with the sliding angles (SAs) being as small as possible, has generated extensive interests.[1–9] Aluminum (Al) and its alloys have been extensively studied due to their wide applications in architecture, transmission lines, electronic elements, and so forth.[10–15] Many studies have been carried out to make Al surfaces superhydrophobic.[16–23] However, the surface tensions of oils and alcohols are in the range of 20–50 mN/m, lower than that of water.[24,25] In general, Young's CAs (defined as the CA on an ideal surface, θ_Y) of oils and alcohols are smaller than 90° on Al surfaces even after being modified by materials having ultra-low surface tensions. We clarified that, from the surface structure point of view, ultra-repellency can only be achieved by appropriate re-entrant surface texture, and the hierarchical micro/nanometer structure which has been

Electronic supplementary material The online version of this article (https://doi.org/10.1007/s11998-017-0012-9) contains supplementary material, which is available to authorized users.

Y. Zhu
Kunming University of Science and Technology, Kunming 650093, China

Y. M. Hu (✉)
College of Engineering, Dali University, Dali 671003, China
e-mail: yongmaohu@163.com

L. Ma, H.-Y.Nie
Surface Science Western, The University of Western Ontario, 999 Collip Circle, London, ON N6G 0J3, Canada

W. M. Lau
Center for Green Innovation, School of Mathematics and Physics, University of Science and Technology Beijing, Beijing 100083, China

commonly used in designing ultra-repellency is one of the re-entrant performances. Therefore, in order to achieve ultra-repellent Al surfaces, a two-step approach is typically required: (1) creation of re-entrant surface textures and (2) modification of the re-entrant textured surfaces with low surface tension materials.

Re-entrant textures can be constructed by the processes of electrospinning,[26,27] anisotropic etching,[26,27] micrometer carbon sphere deposition,[28] carbon sphere template deposition,[29] photolithography, and so on. It is worth mentioning that approaches of the electrochemical process,[30] nanoparticle loading,[31,32] chemical corrosion[33] to superoleophobicity of Al surfaces have been effectively demonstrated. We consider that the function of nanometer structures in the textures mentioned above is to help the transformation of common microstructures to re-entrant structures, or, in other words, all of them have built-in re-entrant surface textures. In order to study the impact of surface structure on the wetting properties, anisotropic etching is a candidate process because of the accurate size control and good reproducibility. However, the instruments required are often expensive, increasing the overall cost. Hence, an accurate surface pattern process of photolithography has advantages.

In the present work, we designed and fabricated re-entrant Al surfaces through a simple approach. Re-entrant micro-pillar-patterned SU-8 surfaces were first prepared, followed by magnetron-sputtering of approximate 70 nm of Al film on top. SU-8 resist is an epoxy-based negative photo-resist which has been widely used to fabricate thick patterns with smooth walls. Patterns made by SU-8 are strong, stiff and chemically stable. Since the thickness of the Al film was too small to influence the morphology of the micro-pillar pattern, the ultimate sample surfaces could be regarded as re-entrant micro-pillar-textured Al surfaces.

In the surface modification strategy, fluoroalkylsilane,[22,34] Teflon,[35] perfluorooctyltriethoxysilane[36] and other molecules have been used to lower the Al surface energy. However, the adhesion between Al and these molecules is limited because there are no chemical bonds formed between the Al substrate and the organic molecules. We have demonstrated that alkyl phosphoric acids, such as dodecylphosphonic acid and octadecylphosphonic acid (OPA), can effectively construct bidentate P–O–Al covalent bonds via a condensation reaction between the hydroxyl of Al and the phosphoric acid headgroups.[6,7] The covalent bonds between Al and the organophosphonic acid headgroups dramatically improved the adhesion, ensuring excellent durability of the composite system.

While alkyl phosphoric acids can effectively modify Al surfaces, the surface energy of densely packed methylene chains and the terminal $-CH_3$ groups is too high to repel oils and alcohols. However, analysis based on a Zisman plot shows that the perfluoroalkyl phosphoric acid (FPA, $CF_3(CF_2)_{13}(CH_2)_2PO(OH)_2$; see Fig. 1a) was able to further lower the surface energy. The critical tension of such a smooth Al surface was lowered to 17.73 mN/m, rendering FPA a good candidate for Al surface modification toward ultra-repellency.

Based on the idea mentioned above, ultra-repellency of Al surfaces was demonstrated via re-entrant micro-pillar texture and FPA modification. These Al surfaces showed an excellent repellency against a wide variety of polar and nonpolar liquids, including water, hexadecane, dodecane, methanol, and ethanol. The robustness of these ultra-repellent surfaces has been discussed and evaluated using failure analysis developed by Tuteja and coworkers.[26]

Experimental

The photolithography process of ~200 μm SU-8 patterns is given as follows: spin-coated on an Si wafer at a speed of 3000 rpm for 20 s, prebaking at 95°C for 1 h, near-UV (400 nm) contacting lithography, postbaking at 95°C for 30 min and development for 20 min in 2-acetoxy-1-methoxypropane (PGMEA, $C_6H_{12}O_3$). The construction of the ultimate re-entrant micro-pillar textured Al surfaces has been depicted elsewhere.[6,7,18,19] The schematic diagram is shown in Fig. 1b.

Crystalline FPA powders (purchased from Specific Polymers, France) were preheated to 100°C prior to use to eliminate moisture. A 1-mM FPA solution in ethanol:tetrahydrofuran (THF) (1:1 ratio) was used to modify the Al surfaces. In the derivatization step, samples with re-entrant textured Al surfaces were immersed in the FPA solution for 2–3 s, followed by ethanol and DI water rinsing and a final N_2 stream drying.

Al surfaces were characterized with CA measurements, scanning electron microscopy (SEM) and X-ray photoelectron spectroscopy (XPS). Readers are referred to the literature,[6,7] for the detailed procedures.

Results and discussion

Surface morphology

In the micrometer scale, SU-8, Al/SU-8 and FPA/Al/SU-8 surfaces showed no obvious difference. For simplicity, Fig. 2 only shows (a) images of the FPA/Al/SU-8 surface and (b) the dimensions of the pillars. The FPA/Al/SU-8 surface exhibited a re-entrant tapered micro-pillar (RTMP) texture with top radius (R), height (H) and inter-pillar gap ($2D$) of 5.1, 19.6, and 14.2 μm, respectively. The feature angle of the textured surface was estimated to be 87.8°. The interface of Al/SU-8 was identified and the thickness of the Al layer was 69 nm. The 69-nm Al layer fully covered the SU-8 surface, ensuring that the final product was FPA-modified RTMP-textured Al surfaces.

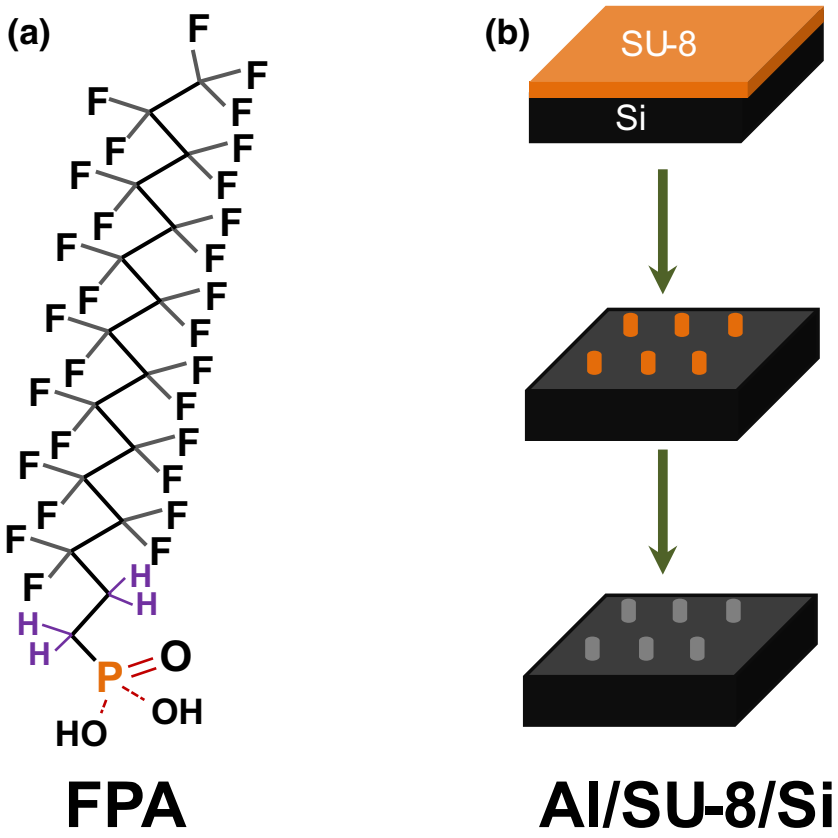

Fig. 1: (a) Molecular structure of FPA used as the modifier in this work and (b) schematic diagram of the fabrication of re-entrant micro-pillar patterned Al surfaces. Re-entrant micro-pillars were first patterned on the SU-8 photoresist surface by photolithography followed by sputtering deposition of Al film

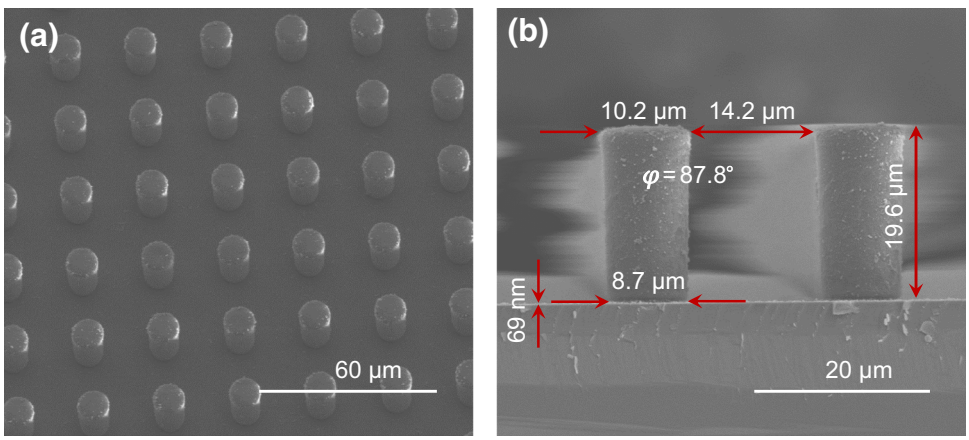

Fig. 2: SEM images of (a) top view and (b) profile of the FPA derivatized Al surfaces. The surfaces exhibit a re-entrant tapered micro-pillar texture with top radius (*R*), height (*H*), distance between two adjacent micro-pillars (2*D*) and feature angle of 5.1 μm, 19.6 μm, 14.2 μm, and 87.8°, respectively

Surface chemistries

Figure 3a shows the XPS spectra of the Al/SU-8 and FPA/Al/SU-8 surfaces. The spectrum of Al/SU-8 agrees well with that of blank Al.[18] In the spectrum of FPA/Al/SU-8, the peaks of phosphorus (P) and fluorine (F) are clearly seen in the binding energy range of 175–200 and 680–695 eV, respectively. The presence of P and F confirmed the FPA derivatization.

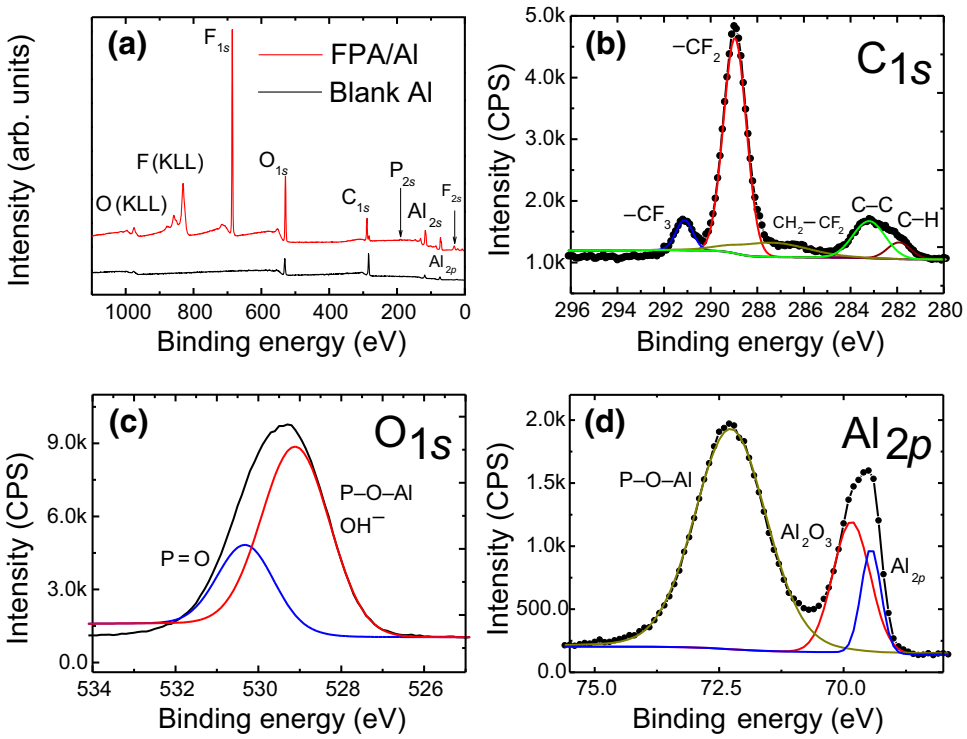

Fig. 3: Survey XPS spectra of blank Al and PFA/Al surfaces (a); (b)–(d) high-resolution XPS spectra of C1s, O1s, and Al2p, respectively

The high-resolution C_{1s} core level spectrum ranging from 280 to 296 eV is shown in Fig. 3b. Five components of $-CF_3$ (291.13 eV), $-CF_2$ (289.00 eV), $-CH_2-CF_2$ (287.41 eV), C–C (283.20 eV) and C–H (281.92) were observed.[37] The concentration of $-CF_3$ estimated from the spectra is 6.38%, well consistent with the theoretical value (6.25%) obtained from the molecular structure of FPA. The successful derivatization of the ultralow surface energy end group of $-CF_3$ (about 6.7 mJ/m^2) on the Al surface was the key to the ultrarepellency.

Multiple curve-fitting solutions were conducted when analyzing the O_{1s} core level lines in Fig. 3c. According to references,[38–41] a reasonable scheme was adopted, in which O_{1s} was de-convoluted into two peaks: a stronger peak at 529.10 eV with FWHM of 1.93 eV represents the main contribution of P-O–Al bonds; another peak at 530.31 eV, with FWHM of 1.58 eV is attributed to P = O bonds. The presence of P = O bonds suggests the bonding configuration of P-O-Al is either mono- or bidentate, rather than tridentate. The O_{1s} line in this spectrum did not show the highest binding energy component at ~538 eV, which is typically observed for organophosphonic acid attached on silicon oxide surfaces through hydrogen bonds or for bulk and multilayers of OPA molecules (which has the same headgroup as FPA) on silicon oxide surfaces.[41] The lack of this component here indicates the FPA layer derivatization on Al surfaces was monolayer. The weight of the integrated intensity of P–O–Al (and –OH) in total O_{1s} intensity was 73.7%, which is higher than the theoretical value of 66.7% for the FPA molecule.

Figure 3d shows an Al metal peak at 69.45 eV, an Al_2O_3 peak at 69.84 eV, and an Al–O bond peak at 72.27 eV. The Al–O bond peak corresponds to the P-O-Al component at 529.10 eV in the O_{1s} peak. The results agree well with the reported peak separation of ~2.8 eV.[39,42]

The bonding energy of the core level peaks of P_{2s}, and F_{1s} were found at 188.80 eV and 686.20 eV, respectively. These results are consistent with those reported by Sarkar and Paynter,[43] suggesting the low surface energy FPA film was successfully assembled on the Al surfaces.

Liquid repellency

We adopted five kinds of liquids to probe the wettability of the FPA-derivatized Al surfaces. They were deionized water (DI water, γ_{lv} = 72.1 mN/m), dodecane (γ_{lv} = 25.4 mN/m), hexadecane (γ_{lv} = 27.5 mN/m), methanol (γ_{lv} = 22.5 mN/m) and ethanol (γ_{lv} = 22.39 mN/m). The CAs of the five liquids on the derivatized Al surfaces are shown in Fig. 4. The derivatized Al surfaces show excellent liquid repellency with static CAs of DI water, dodecane and

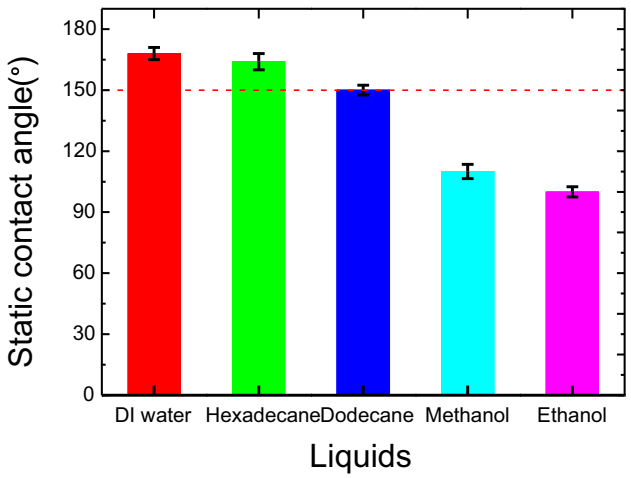

Fig. 4: The CAs of DI water (γ_{lv} = 72.1 mN/m), hexadecane (γ_{lv} = 27.5 mN/m), dodecane (γ_{lv} = 25.4 mN/m), methanol (γ_{lv} = 22.95 mN/m), and ethanol (γ_{lv} = 22.31 mN/m), respectively

hexadecane being larger than 150°. By comparison, the CAs of ethanol and methanol were much smaller, at 110° and 100°, respectively.

The sliding angles (SAs) of DI water, dodecane and hexadecane droplets were below 10°, showing an excellent superamphiphobicity. The SAs of ethanol and alcohols were in the range of 20°–30°. Although the SAs of alcohols were larger than the defined superrepellency requirement of SA < 10°, the as-prepared Al surfaces showed ultra-repellency of a wide variety of liquids.

The impact of the surface texture on liquid repellency

In order to clarify the impact of the surface texture on liquid wettability, we begin the discussion with two widely used wetting regimes, the Wenzel and Cassie–Baxter models, and the free energy of the contacted liquid–solid system. When a liquid droplet is placed on a textured surface, it will stay in either a fully wetted Wenzel state[44] or a solid–liquid–vapor composite contact Cassie–Baxter state.[45] In the Wenzel state, the apparent CA, θ, of a droplet is given by $\cos\theta = r\cos\theta_Y$, where r is the surface roughness ratio defined as the actual surface area divided by the projected surface area, hence $r \geq 1$. Usually, the full liquid–solid contact leads to high CA hysteresis (CAH) which is defined as the difference between the advancing and receding CAs. As a consequence, when liquid droplets move through the solid surfaces, they are actually not really rolling off the textured surface.[44,45] In contrast, a composite interface facilitates both non-wetting (high apparent CA, $\theta > 90°$) and easy droplet rolling-off (low CAH), because of the small liquid–solid contact area.[6–9,46,47] In this state, the apparent CA is given by the Cassie–Baxter equation $\cos\theta = r_f f\cos\theta_Y + f - 1$,[26,48,49] where r_f and f are the roughness ratio and the projected fraction of the wetted area, respectively.

The liquid (droplet)–solid system tends to stay on a state with the minimum overall free energy which is a function of the apparent CA, θ, and the ambient environment. The dimensionless overall free energy, G^*, of a solid–liquid–vapor composite contact system can be written as[48]:

$$G^* = \frac{G}{\gamma_{lv}\pi^{1/3}(3V)^{2/3}} = F^{-2/3}(\theta)[2 - 2\cos\theta - (f)\sin^2\theta] \quad (1)$$

where γ_{lv} is the liquid–vapor interface tension, and V is the total volume of the droplet, and

$$F(\theta) \equiv [2 - 3\cos\theta + \cos^3\theta] \quad (2)$$

$$\Phi(f) \equiv r_f f\cos\theta_Y + f - 1 \quad (3)$$

Equation (1) is established on assumptions that[50,51] (1) the equilibrium shape of the droplet is spherical, and all its distortions are limited to the contact region; (2) the liquid–vapor contact area at the composite interface is quasi planar, thus volume of liquid inside the roughness grooves is negligible; (3) the projected solid–liquid area is approximately equal to the base area of the spherical droplet; and (4) the surveyed total area of the solid surface is a constant and does not affect the minimization of the free energy, hence, it is taken as zero.

Marmur[48] minimized the overall free energy and showed that, for hydrophobic surfaces ($\theta_Y > 90^\circ$), CA (θ) is determined by: (1) the Cassie–Baxter equation in the case of $f \neq 0$ and (2) π in the case of $f = 0$. In addition, the sign of $d^2(r_f f)/df^2$ can be used as a criterion of whether the system is in the Wenzel state or the Cassie–Baxter state.

In order to achieve ultra-repellent surfaces, oils and alcohols with a surface tension smaller than 50 mN/m are often preferred, since, for these liquids, θ_Y is generally smaller than 90° and common rough structures cannot fulfill the requirement.

Figure 5 shows a comparison between two different textured surfaces with the same solid surface energy. When $\theta_Y < 90^\circ < \varphi$ (φ is the feature angle of the local geometry), as shown in Fig. 5a, the net traction, F, originating from the surface tension of the liquid at the liquid–vapor interface is downward, promoting the imbibition of the liquid into the solid texture. A composite liquid–solid interface cannot be sustained and a fully-wetted contact is often the result in this case. On the other hand, if $\varphi \leq \theta_Y < 90^\circ$, as shown in Fig. 5b, F is directed upward and a composite solid–liquid–air interface can be supported. Hence, only re-entrant textured surfaces can support composite liquid–solid–vapor interfaces. It is worth noting that effective surface textures, constructed by electrochem-

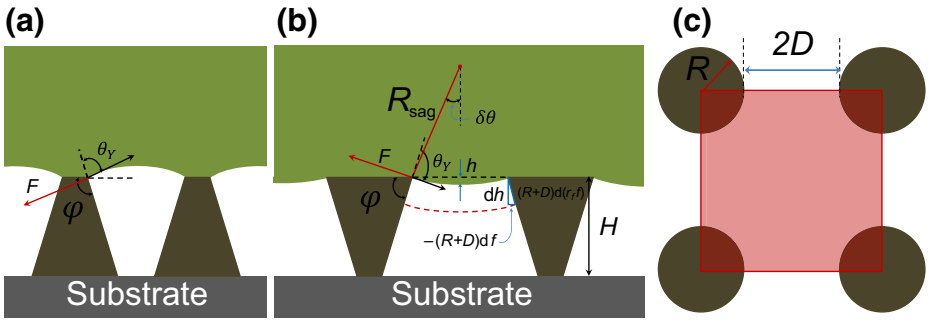

Fig. 5: (a, b) Schematic diagrams of two different solid surfaces having the same surface energy and the same θ_Y, but different geometric angles (φ), and (c) top view of re-entrant micro-pillar pattern

ical processes,[30] nanoparticle loading,[31,32] and chemical corrosion[33] leading to superoleophobicity of Al surfaces, have been reported. On the other hand, straight (not re-entrant) micro-columns with Al surfaces constructed at the same time[16,17] could not repel oils even with FPA modification. We consider that, essentially, the function of the nanostructures in those cases was to help the transformation of the common microstructures to re-entrant structures.

Requirements of a composite interface can also be obtained by minimizing the free energy depicted in equation (1). For FPA-derivatized Al surface texture, the requirements are (1) $\mathrm{d}(r_f f)/\mathrm{d}f = -\cos^{-1}\varphi = -\cos^{-1}\theta_Y$, or $\theta_Y = \varphi$; and (2) In addition, $\mathrm{d}^2(r_f f)/\mathrm{d}f^2 = 0$. In the case of $\theta_Y > 90^\circ$ (e.g., water on flat FPA/Al surface, $\theta_Y = 120^\circ$), the predicted apparent CA $\theta = 180^\circ$. Actually, in the present work, the apparent CA of water is 168°. θ_Y (<90°) are 73.5° and 66.5° for hexadecane and dodecane, respectively, and are too small to be detected for ethanol and methanol. They are all smaller than φ and do not fulfill the relationship of $\theta_Y = \varphi$. However, the system indeed supports a stable composite interface. The differences between the experimental observations and the theoretical predictions are believed to result from three reasons. First, the Al surfaces prepared via sputtering were not perfectly smooth and had nanometer-scale roughness.[18,19] As a consequence, according to the Wenzel regime, the θ_Y values measured were larger (in phobic cases) or smaller (in philic cases) than the theoretical values. Second, the calculation in Figs. 5a and 5b is based on the assumption that the local CA of the composite interface is θ_Y, However, the actual CA will be larger than θ_Y because of the gravity of the droplets. Finally, the liquid–vapor contact area at the composite interface is actually a sagging surface rather than planar (see Fig. 5b).

Evaluation of the as-prepared surface robustness

According to Tuteja and coworkers,[26,27] the robustness of textured liquid repellent surfaces can be evaluated by three parameters: robustness height (H^*), robustness angle (T^*) and robustness factor (A^*). They are related through an equation $1/A^* = 1/H^* + 1/T^*$.

Both robustness parameters of H^* and T^* quantify the sagging and distortion of the liquid–vapor interface as a consequence of the pressure difference across the interface. Such a pressure difference could arise from the application of external pressure, the momentum of a liquid droplet released from a height, or the Laplace pressure within the droplet.[52,53] Considering the diagrams in Fig. 5b, the failure of the composite regime is expected to result from the local sagging of the liquid–vapor interface. The parameter, H^*, provides a dimensionless measurement of the pressure, P_H, required for the sagging height, h, of the liquid–vapor interface to reach the maximum pore depth, H. $H* = P_H/P_{\mathrm{prf}}$, where $P_{\mathrm{ref}} = 2\gamma_{lv}/\ell_{\mathrm{cap}}$ is defined as the characteristic pressure. This is determined by a balance between the surface forces and the body forces acting on the fluid interface. In other words, it is close to the minimum pressure difference across the composite solid–liquid-vapor interface for millimeter-scale droplets or larger puddles on extremely non-wetting, textured surfaces. $\ell_{\mathrm{cap}} = \sqrt{\gamma_{lv}/\rho g}$ is the capillary length of the fluid, ρ the liquid density, and g the acceleration of gravity. For the re-entrant texture shown in Fig. 5b, H^* takes the form:

$$H^* = \frac{P_H}{P_{\mathrm{ref}}} = D^* \frac{H\ell_{\mathrm{cap}}}{D} \tag{4}$$

where $D^* = \frac{2\pi R}{4(D+R)^2 - \pi R^2}$ is defined as the feature size of the system. In the case of water probing of the present textured FPA/Al surfaces, $H^* \approx 403$.

High values of the robustness height H^* represent the formation of a robust composite interface. However, a composite interface with $H^* \gg 1$ can still transit to a fully wetted one because a shift in the local contact angle could happen due to the sagging of the liquid–vapor interface. On any textured surface, the local liquid–vapor interface makes an angle with the solid surface. The liquid–vapor interface becomes more severely distorted with the increase of applied pressure. This distortion causes the liquid–vapor inter-

face to advance downward to a higher value of $\theta = \varphi + \delta\theta$. Any additional pressure will aggravate the distortion. The local vapor–liquid interface can reach the bottom of the re-entrant structure, resulting in a fully wetted interface. In other words, the composite interface transforms into a fully wetted one when the sagging angle reaches $\delta\theta = \theta - \varphi$. Therefore, we can evaluate the robustness pressure (P_θ) required to force a sagging angle of $\delta\theta = \theta - \varphi$. Hence, T^* takes the form:

$$T^* = \frac{P_\theta}{P_{\text{ref}}} = D^* \sin(\theta_Y - \varphi)\ell_{\text{cap}} \tag{5}$$

for water probing in the presence of the Al surface, $T^* \approx 119$. It should be mentioned that for hexadecane, dodecane, ethanol and methanol, Equation (5) cannot be used for an effective evaluation because the values of θ_Y are smaller than φ. We consider the reasons are the same as mentioned in the section on "The impact of the surface texture on liquid repellency."

Any external pressure will cause a simultaneous increase in both the sagging height (h) and the sagging angle ($\delta\theta$). A composite interface will be fully wetted through a combination of the two mechanisms discussed above. Thus, a composite robustness factor, A^*, should be used to evaluate the robustness of composite interfaces. A^* increases with the robustness parameters H^* and T^*. Large values of A^* ($\gg 1$) imply a robust composite interface, corresponding to a high energy barrier between the metastable composite interface and a globally equilibrated, fully wetted one. Small values of A^* (<1) imply that the composite interface cannot maintain its stability against small perturbation such as a small increase of the pressure difference across the liquid–vapor interface.

For the micro-pillar texture, features of R, D, H and φ are defined by the photolithography of SU-8, and the design factors are weakly coupled. Surfaces with both a high apparent contact angle and a highly robust composite interface can be achieved simultaneously. The robustness factor, A^*, of the FPA-derivatized Al surfaces presented in this work was calculated as 92, which is comparable to the values reported by Tuteja et al.,[26] indicating a good robustness.

Conclusions

Re-entrant micro-pillar-textured Al surfaces were fabricated by photolithography of SU-8 and sputtering of Al film. After FPA derivatization, the textured Al surfaces showed ultra-repellency against a wide variety of liquids. The CAs of DI water, hexadecane and dodecane were larger than 150°, and those of methanol and ethanol were above 100°. The SAs of DI water, hexadecane and dodecane droplets were below 10°, showing a desirable superamphiphobicity. The SAs of the alcohols were in the range of 20°–30°.

The robustness height, angle and factors of the ultra-repellent Al surfaces were found to be 403, 119, and 92, respectively, suggesting a good robustness. We believe that optimizing the design parameters of R, D and φ will further improve the robustness factor A^*.

This work has demonstrated that FPA derivatization is effective in lowering Al surface energy. The combination of re-entrant texture and FPA derivatization provides a simple and high throughput approach to ultra-repellence against a wide variety of liquids.

Acknowledgments This study was supported by the National Natural Science Foundation of China (NSFC) (Grant Numbers 11564002 and 11764003), the Scientific Research Fund Project of Yunnan Province Education Department of China (Grant Number 2015Z165), the Scientific Research Fund of Dali University (Grant Number KYBS201301) and the analysis and testing foundation of Kunming University of Science and Technology (Grant Number 2016T20110028). The authors thank Dr. Kar Man Leung for the lithography and sputtering of the substrates.

References

1. Nishino, T, Meguro, M, Nakamae, K, Matsushita, M, Ueda, Y, "The Lowest Surface Free Energy Based on -CF_3 Alignment." *Langmuir*, **15** 4321 (1999)
2. Zisman, W, "A. Relation of the Equilibrium Contact Angle to Liquid and Solid Constitution." *ACS Adv. Chem. Ser.*, **43** 1 (1964)
3. Quéré, D, "Non-sticking Drops." *Rep. Prog. Phys.*, **68** 2495 (2005)
4. Callies, M, Quéré, D, "On Water Repellency." *Soft Mat.*, **1** 55–61 (2005)
5. Quéré, D, "Rough Ideas on Wetting." *Physica A*, **313** 32 (2002)
6. Hu, YM, Zhu, Y, Zhou, Wang, WH, Yi, JH, Xin, SS, He, WJ, Shen, T, "Dip-coating for Dodecylphosphonic Acid Derivatization on Aluminum Surfaces: An Easy Approach to Superhydrophobicity." *J. Coat. Technol. Res.*, **13** 115 (2016)
7. Zhu, Y, Hu, YM, Nie, HY, Zhou, W, Yi, JH, "Superhydrophobicity via Organophosphonic acid Derivatised Aluminium Films." *Surf. Eng.*, **32** 114 (2016)
8. Wang, L, Yang, JY, Zhu, Y, Li, ZH, Shen, T, Yang, DQ, "An Environment-Friendly Fabrication of Superhydrophobic Surfaces on Steel and Magnesium Alloy." *Mater. Lett.*, **171** 297 (2016)
9. Wang, L, Yang, JY, Zhu, Y, Li, ZH, Shen, T, Hu, YM, Yang, DQ, "A Study of the Mechanical and Chemical Durability of Ultra-Ever Dry Superhydrophobic Coating on Low Carbon Steel Surface." *Colloids Surf., A*, **497** 16 (2016)
10. Zheng, S, Li, C, Fu, Q, Hu, W, Xiang, T, Wang, Q, Du, M, Liu, X, Chen, Z, "Development of Stable Superhydrophobic Coatings on Aluminum Surface for Corrosion-Resistant, Self-Cleaning, and Anti-Icing Applications." *Mater. Des.*, **93** 261 (2015)
11. Peng, S, Deng, WA, "Simple Method to Prepare Superamphiphobic Aluminum Surface with Excellent Stability." *Colloids Surf., A*, **481** 143 (2015)

12. Liao, R, Zuo, Z, Guo, C, Yuan, Y, Zhuang, A, ''Fabrication of Superhydrophobic Surface on Aluminum by Continuous Chemical Etching and Its Anti-Icing Property.'' *Appl. Surf. Sci.*, **317** 701 (2014)
13. Saifaldeen, ZS, Khedir, KR, Cansizoglu, M, Demirkan, FT, Karabacak, T, ''Fabrication of Superhydrophobic Surface on Aluminum by Continuous Chemical Etching and Its Anti-Icing Property.'' *J Mater. Sci.*, **49** 1839 (2014)
14. Liu, C, Su, F, Liang, J, ''Facile Fabrication of a Robust and Corrosion Resistant Superhydrophobic Aluminum Alloy Surface by a Novel Method.'' *RSC Adv.*, **4** 55556 (2014)
15. Palanivel, R, Mathews, PK, Murugan, N, Dinaharan, I, ''Effect of Tool Rotational Speed and Pin Profile on Microstructure and Tensile Strength of Dissimilar Friction Stir Welded AA5083-H111 and AA6351-T6 Aluminum Alloys.'' *Mater. Des.*, **40** 7 (2012)
16. Ji, S, Ramadhianti, PA, Nguyen, TB, Kim, W, Lim, H, ''Simple Fabrication Approach for Superhydrophobic and Superoleophobic Al Surface.'' *Microelectron. Eng.*, **111** 404 (2013)
17. Li, XM, Reinhoudt, D, Crego-Calama, M, ''What Do We Need for a Superhydrophobic Surface? A Review on the Recent Progress in the Preparation of Superhydrophobic Surfaces.'' *Chem. Soc. Rev.*, **36** 1350 (2007)
18. Lovenz, H, Despont, M, Fahrni, N, ''High-Aspect-Ratio, Ultrathick, Negative-Tone Near-UV Photoresist and Its Applications for MEMS.'' *Sensor Actuat. A-Phys.*, **64** 33–39 (1998)
19. Lee, KY, LaBianca, NS, Rishten, A, ''Micromachining Applications of a High Resolution Ultrathick Photoresist.'' *J. Vac. Sci. Technol. B*, **13** 3012 (1995)
20. Xu, W, Song, J, Sun, J, Dou, Q, Fan, X, ''Fabrication of Superhydrophobic Surfaces on Aluminum Substrates Using $NaNO_3$ Electrolytes.'' *J. Mater. Sci.*, **46** 5925–5930 (2011)
21. Wu, Y, Zhang, C, ''Analysis of Anti-Condensation Mechanism on Superhydrophobic Anodic Aluminum Oxide Surface.'' *Appl. Therm. Eng.*, **58** 664 (2013)
22. Bernagozzi, I, Antonini, C, Villa, F, Marengo, M, ''Fabricating Superhydrophobic Aluminum: An Optimized One-Step Wet Synthesis Using Fluoroalkyl Silane.'' *Colloids Surf., A*, **441** 919 (2014)
23. Li, P, Chen, X, Yang, G, Yu, L, Zhang, P, ''Fabrication and Characterization of Stable Superhydrophobic Surface with Good Friction-Reducing Performance on Al Foil.'' *Appl. Surf. Sci.*, **300** 184 (2014)
24. Melo-Espinosa, Eliezer Ahmed, Sánchez-Borroto, Yisel, Errasti, Michel, Piloto-Rodríguez, Ramón, Sierens, Roger, Roger-Riba, Jordi, Christopher-Hansen, Alan, ''Surface Tension Prediction Of Vegetable Oils Using Artificial Neural Networks and Multiple Linear Regression.'' *Energy Procedia*, **57** 886 (2014)
25. Song, JL, Huang, S, Hu, K, Lu, Y, Liu, X, Xu, WJ, ''Fabrication of Superoleophobic Surfaces on Al Substrates.'' *J. Mater. Chem. A*, **1** 14783–14789 (2013)
26. Tuteja, A, Choi, W, Mabry, JM, McKinley, GH, Cohen, RE, ''Robust Omniphobic Surfaces.'' *Proc. Natl. Acad. Sci. USA*, **105** 18200 (2008)
27. Tuteja, A, Choi, W, Ma, M, Mabry, JM, Mazzella, SA, Rutledge, GC, McKinley, GH, Cohen, RE, ''Designing Superoleophobic Surfaces.'' *Science*, **318** 1618 (2007)
28. Yu, H, Tian, X, Luo, H, Ma, X, ''Hierarchically Textured Surfaces of Versatile Alloys for Superamphiphobicity.'' *Mater. Lett.*, **138** 184 (2015)
29. Deng, X, Mammen, L, Butt, HJ, Vollmer, D, ''Candle Soot as a Template for a Transparent Robust Superamphiphobic Coating.'' *Science*, **335** 67 (2012)
30. Meng, HF, Wang, ST, Xi, JM, Tang, ZY, Jiang, L, ''Facile Means of Preparing Superamphiphobic Surfaces on Common Engineering Metals.'' *J. Phys. Chem. C*, **112** 11454 (2008)
31. Liu, Y, Cao, HJ, Chen, SG, Wang, DA, ''Ag Nanoparticle-Loaded Hierarchical Superamphiphobic Surface on an Al Substrate with Enhanced Anticorrosion and Antibacterial Properties.'' *J. Phys. Chem. C*, **119** 25449 (2015)
32. Song, JL, Liu, X, Lu, Y, Wu, LB, ''A Rapid Two-Step Electroless Deposition Process to Fabricate Superhydrophobic Coatings on Steel Substrates.'' *J. Coat. Technol. Res.*, **9** 643–650 (2012)
33. Deng, R, Hu, YM, Wang, L, Li, ZH, Shen, T, Zhu, Y, Xiang, JZ, ''An Easy and Environmentally-Friendly Approach to Superamphiphobicity of Aluminum Surfaces.'' *Appl. Surf. Sci.*, **402** 301 (2017)
34. Wu, YP, Zhang, CY, ''Analysis of Anti-Condensation Mechanism on Superhydrophobic Anodic Aluminum Oxide Surface.'' *Appl. Therm. Eng.*, **58** 664 (2013)
35. Jafari, R, Farzaneh, M, ''Fabrication of Superhydrophobic Nanostructured Surface on Aluminum Alloy.'' *Appl. Phys. A*, **102** 195 (2011)
36. Lv, FY, Zhang, P, ''Fabrication and Characterization of Superhydrophobic Surfaces Onaluminum Alloy Substrates.'' *Appl. Surf. Sci.*, **321** 166 (2014)
37. Saleema, N, Sarkar, DK, Paynter, RW, Chen, XG, ''Superhydrophobic Aluminum Alloy Surfaces by A Novel One-Step Process.'' *ACS Appl. Mater. Interfaces*, **2** 2500 (2010)
38. Gouzman, I, Dubey, M, Carolus, MD, Schwartz, J, Bernasek, SL, ''Monolayer vs. Multilayer Self-Assembled Alkylphosphonate Films: X-ray Photoelectron Spectroscopy Studies.'' *Surf. Sci.*, **600** 773 (2006)
39. Hoque, E, DeRose, JA, Hoffmann, P, Mathieu, HJ, Bhushan, B, Cichomski, M, ''Phosphonate Self-Assembled Monolayers on Aluminum Surfaces.'' *J. Chem. Phys.*, **124** 174710 (2006)
40. McIntyre, NS, Nie, HY, Grosvenor, AP, Davidson, RD, Briggs, D, ''XPS Studies of Octadecylphosphonic Acid (OPA) Monolayer Interactions with Some Metal and Mineral Surfaces.'' *Surf. Interface Anal.*, **37** 749 (2005)
41. Hauffman, T, Blajiev, O, Snauwaert, J, van Haesendonck, C, Hubin, A, Terryn, H, ''Study of the Self-Assembling of *n*-Octylphosphonic Acid Layers on Aluminum Oxide.'' *Langmuir*, **24** 13450 (2008)
42. Gredelj, S, Gerson, AR, Kumar, S, Cavallaro, GP, ''Characterization of Aluminium Surfaces With and Without Plasma Nitriding by X-ray Photoelectron Spectroscopy.'' *Appl. Surf. Sci.*, **174** 240 (2001)
43. Sarkar, DK, Paynter, RW, ''One-Step Deposition Process to Obtain Nanostructured Superhydrophobic Thin Films by Galvanic Exchange Reactions.'' *J. Adhesion Sci. Technol.*, **24** 1181 (2010)
44. He, B, Patankar, NA, Lee, J, ''Multiple Equilibrium Droplet Shapes and Design Criterion for Rough Hydrophobic Surfaces.'' *Langmuir*, **19** 4999 (2003)
45. Johnson, RE, Dettre, RH, ''Contact Angle Hysteresis. III. Study of an Idealized Heterogeneous Surface.'' *J. Phys. Chem.*, **68** 1744 (1964)
46. Extrand, CW, ''Model for Contact Angles and Hysteresis on Rough and Ultraphobic Surfaces.'' *Langmuir*, **18** 7991 (2002)
47. Chen, Wei, Fadeev, Alexander Y, Hsieh, Meng Che, Oner, Didem, Youngblood, Jeffrey, McCarthy, Thomas J, ''Ultrahydrophobic and Ultralyophobic Surfaces: Some Comments and Examples.'' *Langmuir*, **15** 3395 (1999)
48. Marmur, A, ''Wetting on Hydrophobic Rough Surfaces: to be Heterogeneous or Not to Be?'' *Langmuir*, **19** 8343 (2003)

49. Michielsen, S, Lee, HJ, ''Design of a Superhydrophobic Surface Using Woven Structures.'' *Langmuir*, **23** 6004 (2007)
50. Wolansky, G, Marmur, A, ''Apparent Contact Angles on Rough Surfaces: the Wenzel Equation Revisited.'' *Colloids Surf. A*, **156** 381 (1999)
51. Randon, S, Haimovich, N, Yeger, E, Marmur, A, ''Partial Wetting Of Chemically Patterned Surfaces: The Effect of Drop Size.'' *J. Colloid Interface Sci.*, **263** 237 (2003)
52. Extrand, CW, ''Criteria for Ultralyophobic Surfaces.'' *Langmuir*, **20** 5013 (2004)
53. Quéré, D, Reyssat, M, ''Non-adhesive Lotus and Other Hydrophobic Materials.'' *Philos. Trans. R. Soc. Lond. A*, **366** 1539 (2008)